



EDINBURGH
INSTRUMENTS








RMS1000 RAMAN MICROSCOPE

Extending the capabilities to Photoluminescence
Microscopy, Time-Resolved Measurements and
Fluorescence Lifetime Imaging (FLIM)

- Truly Confocal
- Five-Position Grating Turrets
- Two Spectrograph Options
- Up to Four Simultaneous Detectors

www.edinst.com

The Raman laser spectrometer ExoMars simulator (RLS Sim): A heavy-duty Raman tool for ground testing on ExoMars

Guillermo Lopez-Reyes¹  | Marco Veneranda¹  | Jose Antonio Manrique¹ |
 Álvaro González Martín¹ | Andoni Moral²  | Carlos Perez-Canora²  |
 Jose Antonio Rodríguez Prieto³ | Aurelio Sanz Arranz¹ | Jesús Saiz Cano¹ |
 Emmanuel Lalla⁴  | Menelaos Konstantinidis⁴ | Olga Prieto-Ballesteros⁵ |
 Jesús Medina¹ | Manuel Ángel González¹ | Elena Charro¹ |
 Jose Manuel Lopez¹ | Fernando Rull¹

¹University of Valladolid (UVa),
Valladolid, Spain

²National Institute of Aerospace
Technology (INTA), Madrid, Spain

³Ingeniería de Sistemas para la Defensa de
España S.A. (ISDEFE), Madrid, Spain

⁴York University, Toronto, Ontario,
Canada

⁵Centro de Astrobiología (INTA), Madrid,
Spain

Correspondence

Guillermo Lopez-Reyes, University of
Valladolid, Av. Francisco Vallés, 8, 47151,
Valladolid, Spain.
Email: guillermo.lopez@uva.es

Funding information

Secretaría de Estado de Investigación,
Desarrollo e Innovación, Grant/Award
Number: PID2019-107442RBC31; H2020
European Commission, Grant/Award
Number: 687302

Abstract

The Raman laser spectrometer (RLS) instrument onboard the Rosalind Franklin rover of the ExoMars 2022 mission will analyze powdered samples on Mars to search for traces of life. To prepare for the mission, the RLS scientific team has developed the RLS ExoMars Simulator (RLS Sim), a flexible model of RLS that operates similarly to the actual instrument, both in laboratory and field conditions, while also emulating the rover operational constraints in terms of sample distribution that are relevant to the Raman analysis. This system can operate autonomously to perform RLS-representative analysis in one or several samples, making it very useful to perform heavy experimental tasks that would otherwise be impossible using a flight-representative model of the instrument. In this work, we introduce the current configuration of the RLS Sim that has incorporated new hardware elements such as the Raman Demonstrator 1 (RAD1) spectrometer with the objective of approaching its performance to that of the actual RLS instrument. To evaluate the scientific capability of the RLS Sim, we have compared it with a replica model of RLS, the RLS Flight Spare (FS). Several acquisition aspects have been evaluated based on the analysis of select samples, assessing the performance in terms of spectral range and resolution and also studying several issues related to the evolution of signal-to-noise ratio (SNR) with different acquisition parameters, especially the number of accumulations. This performance analysis has shown that the RLS Sim in its updated configuration will be a key model to perform support science for the ExoMars mission and the RLS instrument on the

This is an open access article under the terms of the Creative Commons Attribution-NonCommercial-NoDerivs License, which permits use and distribution in any medium, provided the original work is properly cited, the use is non-commercial and no modifications or adaptations are made.

© 2021 The Authors. *Journal of Raman Spectroscopy* published by John Wiley & Sons Ltd.

Rosalind Franklin rover. Designed to work intensively, the use of the RLS Sim in combination with the RLS FS will facilitate maximizing the scientific return of the RLS spectrometer during Martian operations.

KEYWORDS

ExoMars, Raman, RLS, RLS Sim, simulator

1 | INTRODUCTION

The Rosalind Franklin rover onboard ESA ExoMars mission will land on Mars in 2023 carrying a suite of instruments and a drill to perform analysis on samples acquired, for the first time, from down to 2-m depth under the Martian surface.^[1] The analysis of these subsurface samples will increase the probabilities of finding potentially well-preserved organic materials or biosignatures. The drill will extract cores of material that will be characterized by the Mars Multispectral Imager for Subsurface Studies (Ma_Miss), an infrared (IR) spectrometer placed in the rover drill tip,^[2] and the Close-Up Imager (CLUPI), a miniaturized short-range camera system that will picture the sample extracted by the drill.^[3] Then, the material will be powdered by a crusher, while the Sample Preparation and Distribution System (SPDS) will place a flat surface of the powdered sample under the different instruments of the Analytical Laboratory Drawer (ALD) by means of a carousel. The ALD includes three analytical instruments: MicrOmega, an IR spectrometer that will analyze the surface of the samples by illuminating them with an active source of light emitting in different wavelengths^[4]; the Raman Laser Spectrometer (RLS), a Raman spectrometer with excitation wavelength of 532 nm and a spot size of 50 μm that will acquire spectra on several points along the sample surface^[5]; and the Mars Organic Molecule Analyzer (MOMA), a Laser Desorption Mass Spectrometer (MOMA-LDMS) that will analyze the desorbed materials from the sample after shooting it with a laser and also a Gas Chromatography Mass Spectrometer (MOMA-GCMS) to perform detailed desorption analysis on dedicated ovens placed on the rover carousel.^[6] Given that the Rosalind Franklin carousel will allow the analysis by MicrOmega, RLS, and MOMA-LDMS on the same sample surface, it can be stated that the Rosalind Franklin instruments will be able to perform a combined science analysis by interrogating the samples at the very same spot at micrometric scales.^[1,7]

The RLS instrument^[5,8,9] will investigate the samples offered by the rover carousel, acquiring spectra at several spots of the crushed material. As reported previously, the crushing of the samples can induce some undesired

potential effects on the spectra such as a general background increase, peak widening, or even shifting.^[10] In addition, it also eliminates the possibility of assessing the geologic texture and context information of the sample. Thus, the results obtained from RLS (as well as from the other instruments of the ALD) will need to be correlated with those obtained from Ma_Miss and CLUPI, as these will analyze the bulk sample before crushing.^[11]

RLS is designed to automatically adjust the acquisition parameters (e.g., fluorescence quenching time, and integration time) in order to adapt to its operational restrictions, being able to save time in some spots if the spectral quality is above a predefined threshold, as defined in the literature.^[12] The objective is to gather enough data to statistically assess the sample, both qualitatively and quantitatively. To successfully fulfill this task, it is necessary that RLS analyzes a total number of spots per sample ranging between 20 and 39.^[7,12] Indeed, the multipoint acquisition on heterogeneously distributed powdered samples performed by RLS can facilitate the statistical analysis of the data. This results in a detection threshold of minor mineral components in mixtures with a concentration of 1%. This detection threshold does not meet the necessary detection limits as required by the mission for the identification of organics on Mars (established at 10 ppm and lower by the ExoMars mission requirements) but is in line with the requirements for mineralogical identification established for the mission.^[6] Indeed, methodologies have been developed to provide the quantitative estimation of minerals in the samples based only on the Raman spectra obtained in a Rosalind Franklin-like operational scenario.^[11,13–17]

Bearing this in mind, it is of the highest importance to develop systems and instrumentation to allow the characterization of Martian-like materials as well as the development of analytical techniques to obtain the best possible science return from the RLS data on Mars. In this sense, the University of Valladolid has developed the RLS ExoMars Simulator (RLS Sim): a laboratory version of the RLS instrument coupled to a three-axis positioning system emulating the Rosalind Franklin sample positioning carousel.

This system started its development in 2010, with the primary aim of creating and testing the automated

acquisition algorithms and routines that have later been implemented in the flight version of RLS.^[12] In addition, with the capability of automatically positioning the samples, the RLS Sim allows researchers to perform automated analysis resembling the multipoint analysis performed inside the ExoMars rover. To this effect, the software was designed to allow the definition by laboratory technicians (without the need for programming skills) of complex activity plans that use the automatic mode of the instrument, while also has allowed performing combined tests with other instruments such as MicrOmega.^[7]

The potentiality of laboratory systems such as the RLS Sim can be thus addressed from several perspectives:

- 1- Support the development of the RLS instrument: definition and development of the acquisition routines and algorithms of the instrument.^[12]
- 2- Understanding of the analytical capabilities of RLS in the ExoMars rover to help define the operational interface with the carousel and rover: the scientific analysis of powdered samples in a multipoint fashion returned relevant data and information to the definition of the onboard operation mode.^[18–26]
- 3- Preparation for the mission: Investigations on Martian analog samples relevant to the mission's landing site (Oxia Planum) can be carried out with this system both in laboratory and field conditions. These tests are performed jointly with select analysis on the RLS Flight Spare (FS) model, to evaluate the detection capabilities by the instrument with the expected sample types. In addition, by analyzing synthetic samples with known proportions, the simulator data help to create calibration curves that will allow the quantification of mineral abundances in mixtures detected by the instrument once on Mars.^[11,13–17]
- 4- Support during Martian operations: The simulator will play a key role in combination with the Ground Test Model (GTM)—a replica of the rover—and the RLS FS in the support needed during the operations on Mars. The simulator will be used during this time for scientific support (analyzing samples or replicating analysis) which may help interpret and understand the data gathered from RLS. It is important to point out that the RLS Sim is not intended as a substitute or replacement of the RLS FS or GTM nor to provide a fully representative behavior compared with RLS. The objective of this model is to serve as a scientific support tool, able to provide representative data from a scientific point of view, but without the operational complexities associated with a flight instrument such as the RLS FS (temperature, vacuum, data interfaces ...). Being based on commercial components

designed for laboratory conditions working on standard software platforms greatly increases the usability and versatility of the system, facilitating unattended operation and the role of the RLS Sim as a heavy-duty tool for representative scientific data of RLS.

Bearing this in mind, it is of great importance that the RLS Sim emulates the RLS instrument as realistically as possible in terms of the spectral quality of the acquired spectra. Following this logic, the simulator has been upgraded with a laboratory version of the RLS spectrometer, the Raman Demonstrator 1 (RAD1) spectrometer. In this work, we present the results from the performance evaluation of the latest configuration of the RLS Sim, comparing it with the results obtained with a reduced set of selected samples analyzed with the RLS FS Model. In this sense, the spectral range and resolution are compared. In addition, the spectra signal-to-noise ratio (SNR) performance as well as the SNR evolution with respect to the number of accumulations is evaluated in similar samples with the RLS FS and the RLS Sim. This has helped assess the end-to-end representativity of the RLS Sim with respect to the RLS FS (and thus the FM—to which the FS is identical except for its higher laser power) in terms of resolution and SNR. Furthermore, the study on the RLS FS data has helped defining the default optimal acquisition parameters considering the trade-off between spectral quality and time and data bandwidth restrictions, though the final parameters used during Martian operations will be revised after acquisition of representative data from the surface of Mars.

2 | MATERIALS AND METHODS

2.1 | The RLS Sim

The RLS Sim (Figure 1) is a laboratory setup integrated from several hardware and software elements to replicate the behavior of the RLS instrument in cooperation with a positioning mechanism emulating the sample positioning carousel onboard the Rosalind Franklin rover. It is aimed at providing scientific data representative of the RLS instrument when working with the sample positioning of ExoMars.

In order to operate as similarly as possible to RLS, the RLS Sim features a laboratory version of the instrument, the RAD1 spectrometer (Figure 1d), which uses the same diffraction grating as the actual instrument (a 1800 lines per mm transmission grating from Wasatch Photonics), an identical magnification and optical configuration built from commercial components (Pentax SMC 70mm F2.4 collection objective, Nikon 50mm F1.4 focusing

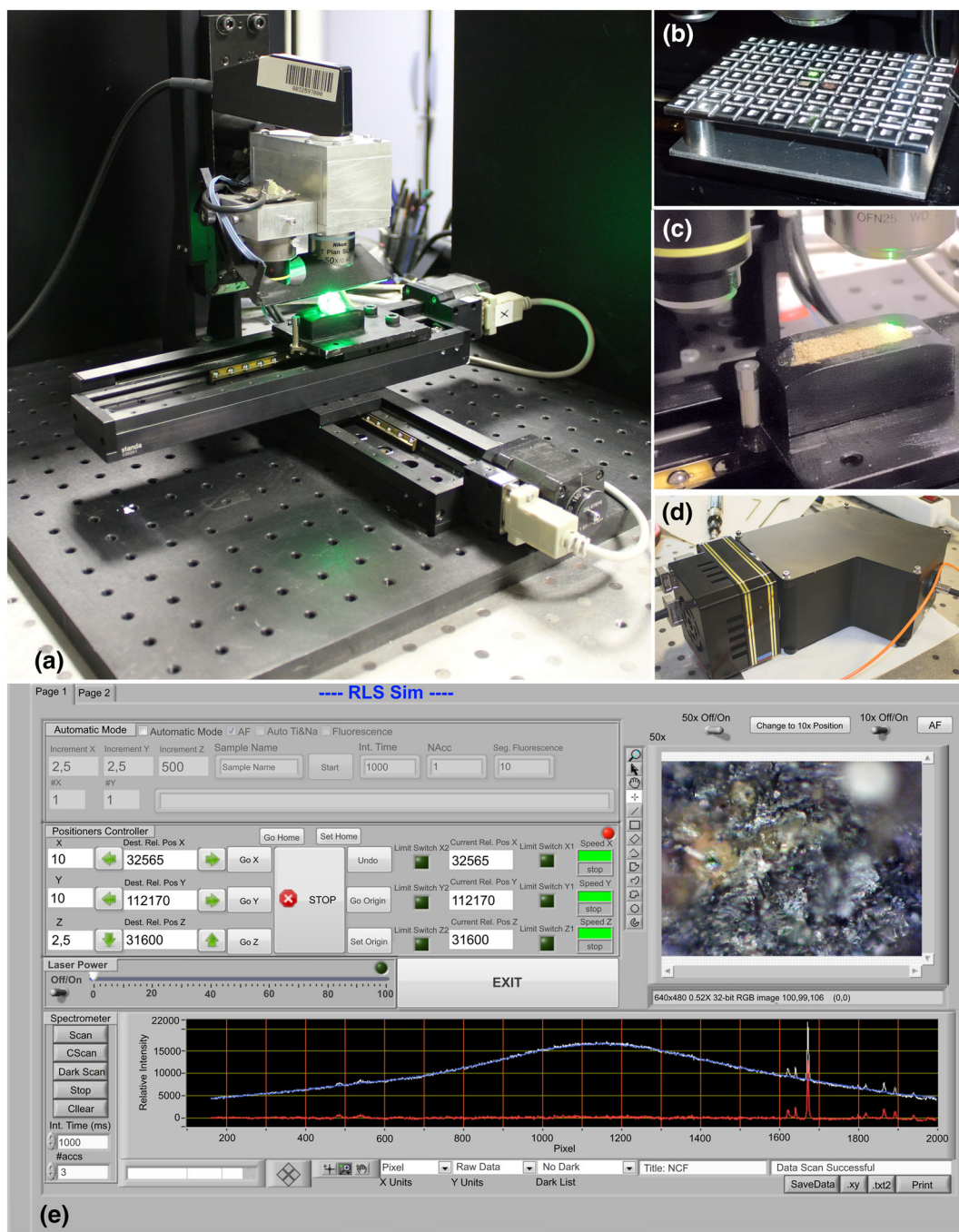


FIGURE 1 The Raman laser spectrometer (RLS) ExoMars Simulator (RLS Sim) (a). Multisample container for automated analysis on multiple samples (b). ExoMars-like sample container (c). RAD1 spectrometer (d). Labview-based control software (e) [Colour figure can be viewed at wileyonlinelibrary.com]

objective), plus a Hamamatsu CCD S10141/1109S with very similar characteristics in terms pixel number and size, dimensions and noise to the flight instrument (refrigerated at -9.5°C , with 2068×512 $12\text{-}\mu\text{m}$ pixels, dark current ~ 15 $e^-/\text{pixel/s}$). The input slit of the spectrometer is, by design, given by the collection fiber core diameter, which is $50\ \mu\text{m}$ for the RLS instrument. This spectrometer has been integrated with the excitation

laser into a case so it can be used both in laboratory experiments but also be safely operated in field conditions for in situ analysis of Martian analogs on Earth.

The Raman acquisition is performed by means of a commercial Spectra Solutions SPS-R532 probe that can be coupled with different fibers. This is very convenient, as this way the RLS Sim can be configured using different collection and excitation fibers, making it quite flexible

and adaptable. However, this implies an extra fiber connection both in the excitation and collection paths, with the associated loss of light compared with a direct fiber coupling. In general, the system is used in two configurations: RLS-like with a 50- or 100- μm core optical fiber and laboratory configuration, with a seven cores round-to-linear 40- μm core fiber, with a round setup on the acquisition side, and a linear arrangement at the spectrometer input. In the latter configuration, the captured light versus spectral resolution trade-off is optimized. However, for this paper, the discussion is centered on the use of one-core fibers to better emulate the RLS instrument performance.

The 532 nm excitation laser is a commercial BWTek BWN-532-100 with 100-mW regulable power with its 105- μm fiber output attached to the Raman probe. The excitation and collection light is focused through a Nikon L Plan SLWD 50X/0.45 EPI objective with a working distance of 27 mm.

The emulation of the RLS autofocus mechanism, as well as the SPDS carousel, is performed by means of a three-axis positioning system Standa Ltd. model 8MT175-200 (x and y axes with 200-mm range to emulate the SPDS) and 8MT175-150 (z axis with 150-mm range for the autofocus mechanism). The motion control is performed using 8SMC5-USB controllers, with a positioning resolution of 2.5 μm in full-step mode (2.5/256- μm steps can also be commanded in microstep mode), which is more than enough to cover the necessary performances (focusing is achieved within $\sim 10\text{-}\mu\text{m}$ resolution; SPDS minimum step on the carousel is $\sim 20\text{ }\mu\text{m}$).

The samples can be placed in an ExoMars-like refillable container with access to a flight-representative calibration target (Figure 1c), but also an 80-sample container can be used to perform automated analysis on multiple samples (Figure 1b).

In addition to these subsystems that emulate the RLS and the rover sample positioning system, the simulator also features equipment to facilitate the operator's work: (1) A joystick allows the manual movement of the positioners. (2) Two cameras to visualize and photograph the sample (though there will not be any on the Rosalind Franklin rover). The 50X objective for laser focusing and Raman light collection is used with a 92/8 pellicle beamsplitter by one of these cameras to exactly visualize the sample spot at the same spatial scale of the acquisition ($280 \times 210\text{ }\mu\text{m}$); the second camera is attached to a Nikon 10X/0.25 Pol objective with 7-cm working distance to facilitate a wider field of view and general evaluation of the sample by the operator. (3) A regulable intensity LED illumination strip is used to illuminate the sample for visualization, which is automatically turned off when the laser is on.

Regarding the operation, the RLS Sim is equipped with a Labview custom-developed software (Figure 1e) that allows manual control over all the elements, data visualization tools, and an automated acquisition mode featuring all the algorithms implemented on the RLS onboard software for acquisition. In addition, an Activity Plan generator has been put in place to allow scientific personnel to program activities without further interaction with the system by a set of preprogrammed code functions, reducing the number of manual tasks and enabling the unsupervised operation of the simulator. The nominal operation of RLS on Rosalind Franklin foresees the acquisition between 20 and 39 spectra along a line of the sample on the refillable container, auto-focusing and auto-adjusting the acquisition parameters at each point to adapt the system to the characteristics of each spot under analysis. The acquisition time is limited to 5 min per point. This whole process is effectively emulated by the RLS Sim, including an image autofocus algorithm based on the gray level variance of the spot region of the image. Furthermore, the simulator allows performing unsupervised acquisition of multiple samples in a row, making it an efficient system for heavy-duty analytical tasks which may last for days or even weeks without interaction with the operator.

2.2 | RLS FS

The RLS instrument Flight Model (FM) was delivered in 2018 and is already integrated in the Rosalind Franklin rover. Given the schedule constraints for delivery, it was not possible to perform a full scientific characterization of the instrument before delivery. These activities were scheduled to be executed with the FS model that was developed following the delivery of the FM. This spare model is a replicate of the actual instrument and is located at the Instituto Nacional de Técnica Aeroespacial (INTA) in Spain.

The RLS instrument is designed to work in the Martian environment (6-mbar CO_2 atmosphere and sub-zero Celsius degrees temperatures). Thus, the RLS FS installation at INTA includes a pressure and temperature chamber in which the spectrometer unit (the most critical in terms of environment) is located to reach the right ambient conditions. This instrument, similar to the FM, features an autofocusing mechanism integrated into the optical head and a fixed-power 532-nm continuous-wave excitation laser providing an irradiance level of around $1\text{ kW}/\text{cm}^2$ (laser power around 20 mW), slightly higher than the actual RLS FM which, by requirement, provides $0.5\text{ kW}/\text{cm}^2$ (12-mW power). The instrument features an E2V detector of $2168 \times 512\text{ }15\text{ }\mu\text{m}$ pixels, cooled down to

−40°C, with a dark current at this temperature of $\sim 45 \text{ e}^-$ /pixel/s.

The operation of this instrument is controlled through the Rover Interface Simulator (RVIS), a system that communicates with RLS using the same communication interface and language that will be used onboard Rosalind Franklin. Also, the activity sequences and control software are similar to those that will be used on Mars.

The FS installation is equipped with a sample positioning system capable of moving powdered samples below the optical head for multipoint analysis in a pseudo-automated way, emulating the work of the SPDS carousel. However, contrary to the RLS Sim, the FS is not deemed for long or demanding analytical activities due to the need for monitorization by operators, maintenance of the adequate environmental conditions and thermal control, preservation of the autofocus motor and laser lifetimes, and so forth. Thus, the scientific evaluation, the mission preparation, and the ExoMars land-site calibration are performed by using a tight RLS FS–RLS Sim tandem in which the RLS Sim is used for heavy-duty tasks, while the RLS FS is saved for select analysis of samples to verify and test calibration models or for the characterization of the instrument performances.

2.3 | Sample selection and spectra acquisition

This work aims to evaluate the performance of the RLS Sim in its current configuration with the RAD1 spectrometer and as described in the previous section, addressing aspects such as spot size, irradiance on the sample, spectral resolution, or SNR on the samples. A Newport LBP-2 Beam profiler has been used to gather the RLS Sim spot size obtained at the sample surface with the 100- μm excitation fiber, as well as with the 50- and 100- μm collection fibers by inserting a white light through the collection optical path. The sample irradiance on the sample plane is subsequently calculated by measuring the output power of the laser at different command values by means of a Coherent LaserCheck power meter, divided by the measured spot size of the excitation on the sample, considering that the expected output power of the RLS instrument is 20 mW. This way the right irradiance level is set on the sample surface by the RLS Sim.

On the one hand, the spectral resolution study was performed based on the analysis of calibration lamps (Kaiser Optical Systems Inc. HoloLab Neon and white lamp generator, and an Ocean Optics HG-1 Mercury and Argon lamp), as well as some bulk or liquid samples

including bulk calcite (CaCO_3 —natural, crystalline), Talc ($\text{Mg}_3\text{Si}_4\text{O}_{10}(\text{OH})_2$ —a phyllosilicate with a very nice peak on the OH region above 3600 cm^{-1}) or cyclohexane (C_6H_{12} —a liquid with very intense Raman bands that is used as Raman calibrant as per norm ASTM E1840).

On the other hand, the SNR assessment and evolution were based on the analysis of geologic standards and samples. Concretely, a set of pure mineral samples in powder form were analyzed by the RLS Sim: (1) diamond (certified 20- to 30- μm grain size powder provided by MicroDiamant AG), (2) Olivine (Forsterite Mg_2SiO_4 —certified by Dillinger Hüttenwerke with reference code SX49-12), (3) Serpentine (antigorite $\text{Mg}_3\text{Si}_2\text{O}_5(\text{OH})_4$ —certified by MINTEK with reference code SARM47), and (4) powdered calcite (CaCO_3 —natural bulk sample crushed with an agate mortar and sieved to obtain a granulometry distribution between 125 and 250 μm).

This sample selection is based upon the good Raman response of the samples (diamond, calcite, cyclohexane, and talc) and their relevance to Mars (olivine is widely present on Mars, with serpentine being one of its main alteration products^[15]) and also directed by the fact that these same batches had previously been analyzed by the RLS FS instrument. No further specific analysis could be performed with the RLS FS for this work, but all the previously acquired data was available for reference, with automatically calculated acquisition times^[12] and variable numbers of accumulations (number of spectra acquired at a determined spot with identical acquisition parameters). These data comprise a total of 5 different sample spots for diamond, 3 of them with 10 accumulations, 1 with 1 accumulation and 1 with 100 accumulations. Olivine and serpentine were acquired in one spot with the RLS FS, with 100 accumulations. Finally, data from three spots of the calcite sample were available with 1, 10, and 100 accumulations, respectively. For the calibration lamps, bulk calcite, and cyclohexane, 1 spectrum with 10 accumulations was needed for each sample/lamp.

All the described samples have been analyzed with the RLS Sim using the automated acquisition algorithms mimicking the RLS acquisition procedures as defined elsewhere^[12] and using the RLS-like collection configuration with one-core fibers. The laser power was set to the representative value of the RLS FS in all cases (20 mW). The analysis of the samples and lamps consisted on the acquisition of at least one spectrum for each sample with auto-adjusted acquisition parameters with each optical configuration (collection fiber with a 50- or 100- μm core). Additionally, at least four spots from diamond, calcite, olivine, and serpentine were acquired, with 1 spot getting 200 accumulations to facilitate the SNR evolution studies.

2.4 | Data analysis

The performance evaluation of both instrument models is addressed first by performing a trade-off between the collection spot size and the expected resolution of the RLS Sim with different collection fibers (cores of 50 and 100 μm), compared with those of the RLS FS. Second, the SNR performance was studied by comparing the absolute SNR performance and its evolution with the number of accumulations.

The spectral resolution is measured based on the full width at half maximum (FWHM) of the Raman bands. For its calculation, the IDAT/SpectPro software was used.^[27–29] This software is a proprietary software being developed by the researchers of the University of Valladolid for the exploitation and analysis of spectra acquired by the RLS instrument. This software includes graphical management and annotation tools (zooming and labeling) and also spectral analytical tools. For example, SpectPro features tools such as a SNR calculator, a baseline removal tool (which can be removed manually in the graphical interface or either automatically calculated to remove the spectrum offset or by using an automated method which defines the baseline at each point by averaging the following n values—being n defined by the user), as well as tools for spectra normalization (by normalizing the maximum to 1 or setting the full intensity span between 0 and 1 or even by normalizing by area) and filtering (featuring Savitsky–Golay and mean filters). Furthermore, SpectPro provides graphical tools to perform peak detection (comparing with a threshold graphically set by the user, providing basic band information such as intensity, position, and FWHM) and band adjustment (allowing the graphical definition of Gaussian–Lorentzian bands to facilitate the deconvolution of bands on complex mixtures).^[27–29] Details on the SpectPro software will be amply discussed in another paper under preparation. For the particular analysis performed with this data, the spectra were processed by removing their baseline, and the peak characteristics were obtained by using the peak detection tool of SpectPro, which directly provides the FWHM of the detected bands.

For the SNR performance study, it has to be considered that the objective of this work is to configure and parameterize the RLS Sim operation to obtain the most similar performance to that of the RLS FS in terms of the acquired spectral quality and resolution, as these two aspects will limit the scientific capabilities of the instrument. Taking this into account, the SNR evaluation has been performed end-to-end, without considering or aiming at getting identical photon budgets throughout the optical chain. Instead, the objective was to ensure

(1) a similar spot size and irradiance on the sample, (2) obtaining representative spectra in terms of resolution, and (3) adjusting the operational parameters (mainly the number of accumulations) to ensure a final similar SNR on the same samples.

The SNR performance and evolution with the number of accumulations were calculated by using routines created ad hoc for this analysis. The rigorous definition of SNR is the inverse of the relative standard deviation of the measurement,^[30] that is, the peak height average of several consecutive acquisitions divided by its standard deviation. However, this definition is not as useful to provide an idea of the spectral quality of the spectrum but of the acquisition device (as it measures the peak intensity variation along several acquisitions). Also, it is not very practical as it needs several spectra to obtain only one SNR value. Thus, an alternative definition of SNR is used in this work, where $\text{SNR} = I_{\text{peak}}/\sigma_{200}$, in which the main peak intensity (I_{peak}) is divided by the standard deviation of the points on a 200 cm^{-1} region of the spectrum with no Raman bands (σ_{200}). This way it is possible to evaluate the capability to distinguish a peak from the spectral random variations or noise.

In our analysis we use the second definition of SNR and calculate it using a difference spectra method: the difference between two consecutively acquired spectra is calculated to obtain a noise spectrum (as the subtraction is removing all the nonrandom elements on the spectra such as the baseline or the Raman bands). This spectrum is used to calculate the standard deviation of the noise (σ_{200}) in a predefined Noise Region of 200 cm^{-1} , a spectral range with enough data points to ensure that the final SNR value is approximately the same irrespective of the selected noise region. The selected noise regions for the different materials are gathered in Table 1.

Additionally, the spectrum intensity is calculated as the maximum value of the desired peak with respect to the baseline, defined as the straight line between the extremes of a predefined Peak Region (Table 1). The SNR is then calculated as the quotient between the calculated intensity and noise.

This SNR calculation approach has the advantage of not considering the inherent uncertainty introduced by baseline correction methods. However, the effectivity of the method is compromised due to the need of using two spectra to calculate the noise spectrum, reducing the effective number of available spectra for analysis. Also, this method reduces the actual noise by a factor of $\sqrt{2}$ due to the subtraction operation.^[30] Thus, this bias is corrected for by multiplying the results of the SNR calculation by a factor $\sqrt{2}$.

To obtain the SNR calculation evolution for different numbers of accumulations, the spectra with one

TABLE 1 Signal and noise ranges used for the SNR analysis for each sample

	Signal region (cm ⁻¹)	Noise region (cm ⁻¹)
Calcite	1025–1150	1175–1375
Diamond	1200–1400	1600–1800
Olivine	750–1000	105–1250
Serpentine	310–430	1200–1400

Abbreviation: SNR, signal-to-noise ratio.

accumulation, are averaged in disjoint sets, obtaining at least two spectra with the same number of accumulations. This way, the difference spectra method can be applied to calculate the SNR with each accumulation number. Then, the SNR evolution with respect to the accumulation number is depicted for comparison and adjusted to a potential function.

3 | RESULTS AND DISCUSSION

3.1 | Excitation spot size and sample irradiance level

The RLS Sim laser output fiber measurement directly coupled to the optical head provides a measured spot size on the sample with an average diameter of 51 μm . This value correlates very well with the spot size of the RLS FM and FS instruments (50 μm). Considering this, the same sample irradiance level is obtained by setting the laser to a power output similar to that of the RLS FS (around 20 mW), resulting in an average irradiance on the sample surface of 1KW/cm². This value is higher than the expected irradiance value for RLS FM, but similar to that of the RLS FS, allowing the direct comparison between RLS FS and RLS Sim. However, it has to be considered that the RLS Sim's capability of adjusting the laser power also allows getting the same irradiance levels similar to those of the RLS FM.

3.2 | Spectral range, collection spot size, and spectral resolution

The spectral range and resolution are key parameters to determine the capabilities and quality of the acquired spectra of a spectrometer. The RLS instrument was designed to obtain a spectral range between 0 and 3800 cm⁻¹. This spectral range is amply covered by the RAD1 spectrometer integrated in the RLS Sim, with spectral ranges expanding further than 0 to 4000 cm⁻¹.

The RLS spectrometer unit has a resolution requirement of 6 to 8 cm⁻¹.^[5] Nevertheless, experimental results for both the FS and FM have shown that the resolution is worse than these values in end-to-end analysis due to defocusing in the lower spectral region (Table 2). This is related to temperature and other operational/handcraft issues that will be detailed in a dedicated paper.

In order to evaluate the RLS Sim configuration best fitting the RLS actual resolution, we performed tests with the two different core size fibers (50 and 100 μm) and measured both the spot size and effective resolution with different bands in different spectral regions from the calibration lamps and some selected bands from calcite, cyclohexane, diamond, and talc to cover the spectral range homogeneously. Comparing these values (see Table 2) with those obtained with the RLS FS for the same bands (Figure 2), it is observed that the RLS FS resolution is not constant throughout the whole spectral range, showing some defocusing on the spectral region below 1400 cm⁻¹. When comparing the FS values with both optical configurations of the RLS Sim, it can be observed how the 50- μm fiber fits quite well the results on the region above 1400 cm⁻¹, while the 100- μm fiber seems to fit best the lower spectral region, clearly underperforming the FS in the higher region.

The RLS Sim needs to work in one optical configuration only as it is not possible to use different fibers for different spectral regions. In general, most Raman lines are found on the shorter wavenumber regions, and considering that these are usually narrower than those on the higher spectral regions, it seems reasonable to favor the configuration most resembling the RLS FS on this region, thus selecting the configuration with the 100- μm fiber. This configuration will negatively affect the detection capabilities of the RLS Sim on the regions above 1400 cm⁻¹, but this will ensure that the performance with the RLS Sim will always be similar or worse than that of the FS, which is desirable to be able to understand the scientific capabilities of the RLS instrument on the surface of Mars, given the similarity between the RLS FS and FM.

3.3 | SNR performance and evolution with accumulations

The key parameter to address the spectral quality beyond spectral resolution is the achievable SNR of the spectrum, calculated with the alternative definition of SNR previously described. The SNR values for the RLS Sim and the RLS FS obtained for the different geologic standards and samples described in the materials and methods section have been compared. As shown in Figure 3 the

TABLE 2 Measured FWHM for several bands from samples and noble gas lamps distributed along the spectral range for the RLS FS and the RLS Sim with 50- and 100- μm collection optical fibers

Light source or sample	Raman band wavenumber (cm^{-1})	Measured FWHM (cm^{-1})		
		RLS FS	RLS Sim (100 μm)	RLS Sim (50 μm)
Calcite	281	26.6	25.5	19.1
Hg-Ar	494	19.7	21.0	--
Calcite	712	25.4	21.6	12.8
Cyclohexane	812	27.5	21.5	13.2
Cyclohexane	1036	31.7	26.6	19.9
Calcite	1086	17.9	19.1	10.8
Cyclohexane	1275	27.4	26.1	19.1
Diamond	1332	17.4	19.6	11.1
Hg-Ar	1472	11.1	17.5	9.1
Hg-Ar	1534	10.5	17.3	9.0
Ne	1715	9.3	17.6	8.4
Calcite	1749	13.7	20.3	12.4
Ne	1803	9.3	17.2	8.4
Ne	1982	8.8	16.8	8.2
Ne	2067	8.1	17.0	8.5
Ne	2218	7.4	16.8	9.3
Ne	2340	7.9	17.1	9.4
Ne	2400	9.1	16.7	9.7
Ne	2523	9.1	16.7	9.6
Ne	2578	8.1	16.3	9.0
Ne	2719	8.0	15.8	8.2
Ne	2845	7.9	15.5	7.8
Ne	2941	7.7	15.1	6.9
Ne	3014	8.6	15.1	7.2
Ne	3136	8.2	14.9	6.9
Ne	3182	8.4	14.8	7.1
Ne	3432	8.9	14.6	7.3
Ne	3494	8.0	14.3	6.7
Ne	3647	7.8	13.9	6.8
Talc	3639	8.5	16.1	7.3
Ne	3826	8.3	13.8	6.5
Ne	3913	7.3	13.5	6.25

Abbreviations: FWHM, full width at half maximum; RLS FS, Raman laser spectrometer Flight Spare; RLS Sim, Raman laser spectrometer ExoMars Simulator.

RLS FS SNR does not present a distribution for olivine and serpentine, as there is only one point for each of these samples. However, for calcite and diamond, the SNR dispersion among different points is higher in the RLS FS compared with the RLS Sim. This is due to the different conditions in which the spectra were acquired. While the data from the RLS Sim were collected on the same sample batch in one acquisition session, the

different spots obtained with the RLS FS were obtained in different sessions executed with weeks or even months between them, which could explain the higher variability of the final spectral quality. Furthermore, given that the samples were analyzed in different spots by both instruments, the absolute SNR values cannot be directly compared between spots. However, the statistical distribution for different spectra of the same sample shows a general

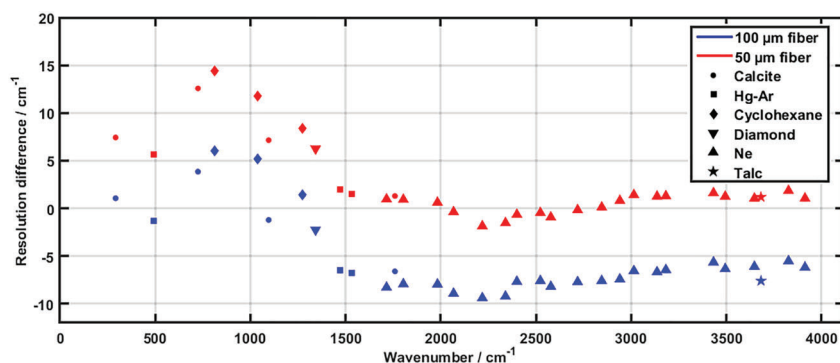


FIGURE 2 Resolution difference between the Raman laser spectrometer Flight Spare (RLS FS) and the RLS Sim with 100 μm (blue) and 50 μm (red) core fibers. Negative values show underperformance regions of the RLS Sim compared with the RLS FS. A value of 0 indicates similar performance in terms of spectral resolution [Colour figure can be viewed at [wileyonlinelibrary.com](#)]

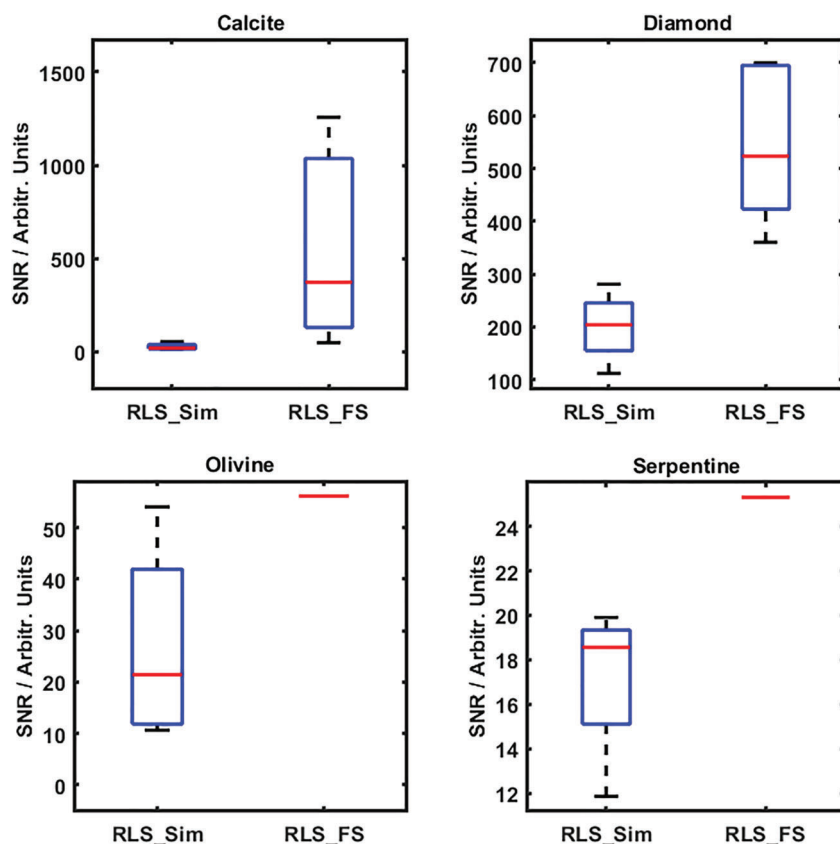


FIGURE 3 Signal-to-noise ratio (SNR) distribution for different materials analyzed with the Raman laser spectrometer (RLS) Sim and the RLS Flight Spare (FS). The box plots represent the median value for all the points (red line) and the four quartiles (blue box and black whiskers) [Colour figure can be viewed at [wileyonlinelibrary.com](#)]

underperformance by the RLS Sim compared with the RLS FS, which can also be observed in the olivine example in Figure 4. This is explained by the losses suffered on the collection optical path due to the collection fiber connectors to the optical head, which effectively reduce the incoming light to the spectrometer compared with the RLS FS. This issue is clearly observed in the excitation path, with the output laser power on the sample being significantly lower compared with other Raman probes with direct fiber coupling.

There are two operational parameters that can be used to increase the spectral quality of the acquired spectra: the integration time and the number of accumulations. As described elsewhere,^[12] instruments with

cooled detectors such as the RLS improve the SNR more with the integration time than with the number of accumulations. However, it is only possible to increase the integration time as long as the detector does not saturate, limiting the maximum time that can be used to acquire an individual spectrum. Both the RLS FS and RLS Sim models implement the automatic calculation of the integration time to ensure the maximum signal quality without saturating the spectrometer detector, so there is no further margin to improve with this parameter. On the other hand, the number of accumulations also affects the SNR of the final acquired spectra. Figure 4 shows an example of the evolution of the spectra of the olivine sample with different numbers of accumulations where

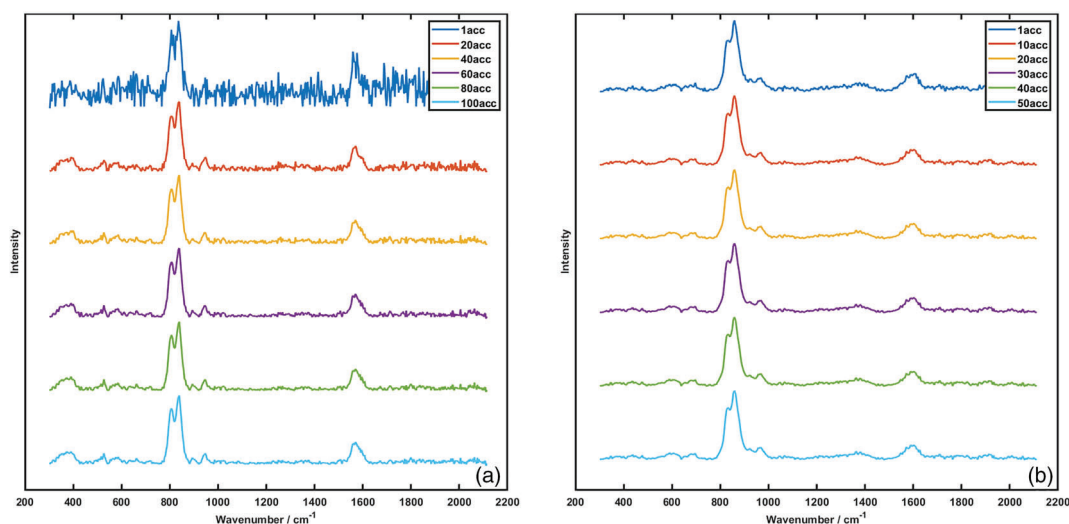
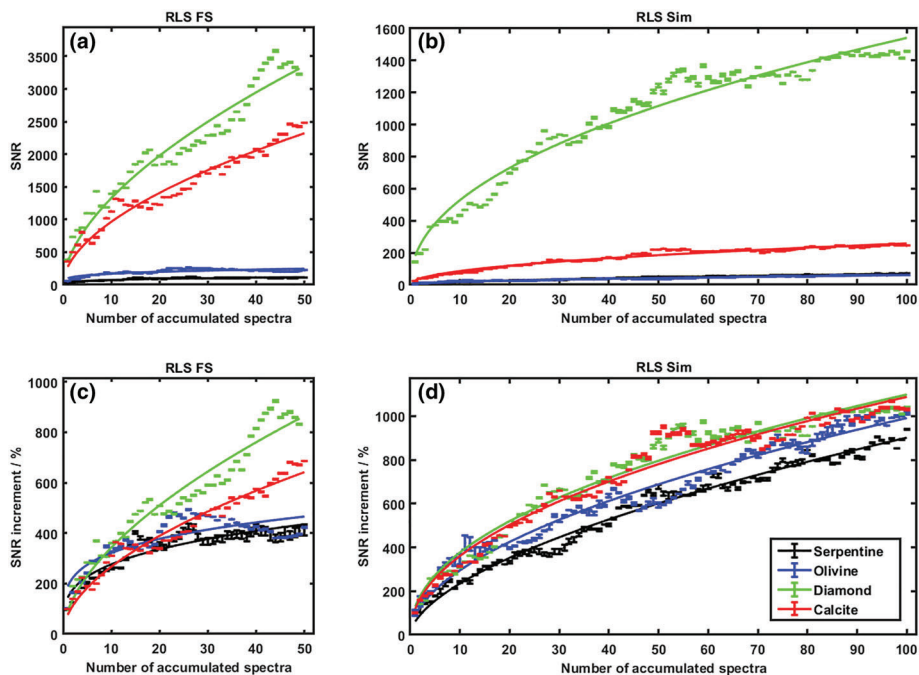


FIGURE 4 Spectra evolution for different numbers of accumulations on an olivine sample. Raman laser spectrometer (RLS) Sim (a) and RLS Flight Spare (FS) (b) [Colour figure can be viewed at [wileyonlinelibrary.com](#)]

FIGURE 5 Signal-to-noise ratio (SNR) evolution with increasing numbers of accumulations for the Raman laser spectrometer Flight Spare (RLS FS) (a) and RLS ExoMars Simulator (Sim) (b). SNR increment evolution with increasing numbers of accumulations for the RLS FS (c) and RLS Sim (d) [Colour figure can be viewed at [wileyonlinelibrary.com](#)]



the spectral quality improvement is qualitatively observed.

The evolution of the SNR with accumulations (Figure 5a,b) quantitatively shows how the accumulation process implies a general improvement of the SNR of the acquired spectra for the different samples. This result is in consonance with the qualitative impression from Figure 4 and the theory: Spectra accumulation improves the standard deviation of the noise by averaging the random noise components, resulting in better SNR values.

Also, these graphs can be used to compare the absolute SNR values obtained for the different materials and

instruments. This comparison can be biased by the different acquisition configurations and uncertainty in the analysis due to the powder form of the analyzed samples. Nevertheless, it can be observed how, in general, the SNR values ratio among the different materials is consistent between both instruments, with diamond and calcite performing much better than olivine and serpentine, as explained by their different cross-section values which make Raman emission of diamond and calcite much more probable than on the others.

The examination of the relative SNR increment in % (calculated with respect to the one-accumulation

spectrum; see Figure 5c,d) shows a more consistent and predictable behavior of the RLS Sim when comparing the SNR increment evolution for the different samples. This can be explained by the fact that the RLS Sim is designed and built to work in a laboratory environment, while the RLS FS is designed to work under Martian conditions. As these Martian conditions cannot be perfectly replicated on ground, there is higher instability on the thermal control of the RLS FS which in turn explains the observed variations of the SNR increment curve.

The representation in Figure 5c is very useful to assess the trade-off between increasing the number of accumulations for higher spectral quality and the operational resources consumed on Mars (which are very limited). In this sense, there is a wide agreement among all parties in the RLS development project to configure the instrument number of accumulations for Martian operations to maximize the data's scientific quality and carefully assess the impact on the operational budgets. Bearing this in mind, the criterion has been to establish the default number of accumulations for Martian operations in a value of 20, which is the value in which the SNR increment curve bends down reducing the actual SNR increment with respect to the increase observed in the lineal region of the curve. This is especially noticeable in the lower SNR samples (olivine and serpentine). This value provides a good enough SNR increase with each new accumulation, while being consistent with the data volume, bandwidth, and operation time restrictions for the RLS instrument.

Finally, it is important to stress again the reduced performance of the RLS Sim compared with the RLS FS. On the one hand, even if the sample-related uncertainty prevents a very precise comparison of the obtained absolute SNR values, it can be estimated that the RLS Sim SNR is, on average, between two and three times worse than the RLS FS (see Figure 3). On the other hand, the approximate average SNR increment for 20 accumulations on the RLS FS is around four times the one-accumulation spectrum (see Figure 5c). If we consider the SNR increment of the RLS Sim (Figure 5d), we observe a steady increase of SNR with the number of accumulations. Thus, it is possible to partially compensate for the reduced performance of the RLS Sim with higher numbers of accumulations. This will penalize the acquisition times and budgets on the analysis performed by the RLS Sim, but there are no constraints in this regard. This way, by acquiring spectra with 80 accumulations on the RLS Sim, the spectra SNR is increased between 8 and 10 times depending on the sample, which would compensate spectra with SNR between 2 and 2.5 times less than those acquired with 20 accumulations (average increase of 4 times) on an equivalent sample with the RLS FS. With

this configuration the RLS Sim will be able to approach the RLS performance without overperforming, which is of paramount importance to be able to use the RLS Sim to understand the RLS instrument's scientific capabilities during Martian surface operations.

4 | CONCLUSIONS

An analysis performed with the RLS Sim has been presented, studying aspects such as the acquisition of spectra on different samples, evaluating the spectral resolution or the SNR performance on this model, compared with the RLS FS. The rationale behind the use of the RLS Sim is to have a laboratory model that can obtain scientifically representative data compared with the RLS instrument onboard the Rosalind Franklin rover, without enduring the operational complexities associated with a flight-like instrument such as the RLS FS.

The RLS Sim has been updated for representativity with the RAD1, a custom-built spectrometer with very similar characteristics to those of RLS, but assembled from commercial optics, hardware, and software components. In this work, we have presented analyses performed with the RLS Sim to study the best optical configuration of the system compared with the RLS FS in terms of spectral resolution. In this regard, the RLS Sim has been configured to obtain an excitation spot size with the same irradiance levels provided by the RLS FS. On the other hand, the collection path is configured to emulate the performance on the lower wavenumbers region, even though this implies a worse resolution on the higher spectral region. This is done to ensure that the performance of the RLS Sim is always kept equal or worse than the RLS FS, as the final objective of the RLS Sim is to help understand the potential scientific return from the RLS instrument on Mars.

The SNR performance study on the RLS Sim has been compared with the RLS FS, showing a significant underperformance by the RLS Sim compared with the FS, mostly due to fiber connector-related losses on the optical head collection path. The SNR evolution versus the number of accumulations has allowed showing a coherent behavior when comparing the RLS FS results with the RLS Sim ones, with some differences that can be linked to the uncertainties introduced by the fact that samples are powdered and the spot size is in the order of the mineral grain size. However, the SNR evolution with the number of accumulations shows that the RLS Sim underperformance can be greatly compensated by increasing the number of accumulations for the RLS Sim.

Concretely, the analysis of RLS FS data has provided insights as to what would be an adequate default

parameter for the number of accumulations to be acquired by RLS during Martian operations, though it will probably need to be refined after arrival to Mars. All in all, it can be concluded that the described configuration of the RLS Sim provides a good approximation to the behavior of the real instrument, and thus, the RLS Sim will be a key tool for the preparation and support of Martian operations. Indeed, the RLS Sim is a very flexible tool for the analysis of samples in operational conditions similar to those of the actual RLS instrument on Rosalind Franklin, as it acquires spectra using the same acquisition algorithms as RLS and also emulates the sample positioning of the Rosalind Franklin carousel. In addition, RLS Sim allows the sequential analysis of up to 80 samples in a laboratory environment, therefore facilitating the unsupervised heavy-duty use of this instrument to characterize the instrument and landing site of the Rosalind Franklin rover. Furthermore, the RLS Sim acquisition system is designed to be resilient to open environments, making it suitable for in situ analysis of Martian analogs on Earth.

Bearing this in mind, using the RLS Sim for heavy-duty analysis in combination with selected analysis on the RLS FS is a powerful strategy to prepare the RLS instrument and team for the ExoMars mission. Additionally, it will also be key during Mars operations given its capability of automatically obtaining data in an operationally representative scenario, making the RLS Sim a key tool to support the Martian operations of the RLS instrument onboard ExoMars.

ACKNOWLEDGMENTS

The authors thank the Secretaría de Estado de Investigación, Desarrollo e Innovación through grant PID2019-107442RBC31 and the H2020 European Commission through grant 687302.

DATA AVAILABILITY STATEMENT

The data that support the findings of this study are available from the corresponding author upon reasonable request.

ORCID

Guillermo Lopez-Reyes  <https://orcid.org/0000-0003-1005-1760>

Marco Veneranda  <https://orcid.org/0000-0002-7185-2791>

Andoni Moral  <https://orcid.org/0000-0002-6190-8560>

Carlos Perez-Canora  <https://orcid.org/0000-0002-9575-1258>

Emmanuel Lalla  <https://orcid.org/0000-0002-0005-1006>

REFERENCES

- [1] J. L. Vago, F. Westall, A. J. Coates, R. Jaumann, O. Korablev, V. Ciarletti, I. Mitrofanov, J. L. Josset, M. C. De Sanctis, J. P. Bibring, F. Rull, F. Goesmann, H. Steininger, W. Goetz, W. Brinckerhoff, C. Szopa, F. Raulin, H. G. M. Edwards, L. G. Whyte, A. G. Fairén, J. Bridges, E. Hauber, G. G. Ori, S. Werner, D. Loizeau, R. O. Kuzmin, R. M. E. Williams, J. Flahaut, F. Forget, D. Rodionov, H. Svedhem, E. Sefton-Nash, G. Kminek, L. Lorenzoni, L. Joudrier, V. Mikhailov, A. Zashchirinskiy, S. Alexashkin, F. Calantropio, A. Merlo, P. Poulakis, O. Witasse, O. Bayle, S. Bayón, U. Meierhenrich, J. Carter, J. M. García-Ruiz, P. Baglioni, A. Haldemann, A. J. Ball, A. Debus, R. Lindner, F. Haessig, D. Monteiro, R. Trautner, C. Volland, P. Rebeyre, D. Gouly, F. Didot, S. Durrant, E. Zekri, D. Koschny, A. Toni, G. Visentin, M. Zwick, M. Van Winnendael, M. Azkarate, C. Carreau, *Astrobiology* **2017**, *17*, 471.
- [2] M. C. De Sanctis, F. Altieri, E. Ammannito, D. Biondi, S. De Angelis, M. Meini, G. Mondello, S. Novi, R. Paolinetti, M. Soldani, R. Mugnuolo, S. Pirrotta, J. L. Vago, the Ma_MISS team, *Astrobiology* **2017**, *17*, 612.
- [3] J. L. Josset, F. Westall, B. A. Hofmann, J. Spray, C. Cockell, S. Kempe, A. D. Griffiths, M. C. De Sanctis, L. Colangeli, D. Koschny, K. Föllmi, E. Verrecchia, L. Diamond, M. Josset, E. J. Javaux, F. Esposito, M. Gunn, A. L. Souchon-Leitner, T. R. R. Bontognali, O. Korablev, S. Erkman, G. Paar, S. Ulamec, F. Foucher, P. Martin, A. Verhaeghe, M. Tanevski, J. L. Vago, *Astrobiology* **2017**, *17*, 595.
- [4] J. P. Bibring, V. Hamm, C. Pilorget, J. L. Vago, and the Micro-mega Team, *Astrobiology* **2017**, *17*, 621.
- [5] F. Rull, S. Maurice, I. Hutchinson, A. Moral, C. Perez, C. Diaz, M. Colombo, T. Belenguer, G. Lopez-Reyes, A. Sansano, O. Forni, Y. Parot, N. Striebig, S. Woodward, C. Howe, N. Tarcea, P. Rodriguez, L. Seoane, A. Santiago, J. A. Rodriguez-Prieto, J. Medina, P. Gallego, R. Canchal, P. Santamaría, G. Ramos, J. L. Vago, *Astrobiology* **2017**, *17*, 627.
- [6] F. Goesmann, W. B. Brinckerhoff, F. Raulin, W. Goetz, R. M. Danell, S. A. Getty, S. Siljeström, H. Mißbach, H. Steininger, R. D. Arevalo Jr., A. Buch, C. Freissinet, A. Grubisic, U. J. Meierhenrich, V. T. Pinnick, F. Stalport, C. Szopa, J. L. Vago, R. Lindner, M. D. Schulte, J. R. Brucato, D. P. Glavin, N. Grand, X. Li, F. H. W. van Amerom, and the MOMA Science Team, *Astrobiology* **2017**, *17*, 655.
- [7] G. Lopez-Reyes, C. Pilorget, A. G. Moral, J. A. Manrique, A. Sanz, A. Berrocal, M. Veneranda, F. Rull, J. Medina, V. Hamm, J. Bibring, J. A. Rodriguez, C. Perez Canora, E. Mateo-Marti, O. Prieto-Ballesteros, E. Lalla, J. L. Vago, *J. Raman Spectrosc.* **2020**, *51*, 1718.
- [8] A. G. Moral, F. Rull, S. Maurice, I. B. Hutchinson, C. P. Canora, L. Seoane, G. López-Reyes, J. A. Rodriguez Prieto, P. Rodriguez, G. Ramos, Y. Parot, O. Forni, *J. Raman Spectrosc.* **2019**, *51*, 1771.
- [9] G. Ramos, M. Sanz-Palomino, A. G. Moral, C. Pérez, T. Belenguer, R. Canchal, J. A. R. Prieto, A. Santiago, C. Gordillo, D. Escribano, G. Lopez-Reyes, F. Rull, *J. Raman Spectrosc.* **2019**, *51*, 1761.
- [10] F. Foucher, G. Lopez-Reyes, N. Bost, F. Rull-Perez, P. Rüßmann, F. Westall, *J. Raman Spectrosc.* **2013**, *44*, 916.

- [11] G. Lopez-Reyes, F. Rull, G. Venegas, F. Westall, F. Foucher, N. Bost, A. Sanz, A. Catalá-Espí, A. Vegas, I. Hermosilla, A. Sansano, J. Medina, *Eur. J. Mineral.* **2013**, *25*, 721.
- [12] G. Lopez-Reyes, F. Rull Pérez, *J. Raman Spectrosc.* **2017**, *48*, 1654.
- [13] M. Veneranda, G. Lopez-Reyes, J. A. Manrique-Martinez, A. Sanz-Arranz, E. Lalla, M. Konstantinidis, A. Moral, J. Medina, F. Rull, *Sci. Rep.* **2020**, *10*, 16954.
- [14] M. Veneranda, G. Lopez-Reyes, J. A. Manrique, J. Medina, P. Ruiz-Galende, I. Torre-Fdez, K. Castro, C. Lantz, F. Poulet, H. Dypvik, S. C. Werner, F. Rull, *Astrobiology* **2020**, *20*, 349.
- [15] M. Veneranda, G. Lopez-Reyes, E. Pascual Sanchez, A. M. Krzesińska, J. A. Manrique-Martinez, A. Sanz-Arranz, C. Lantz, E. Lalla, A. Moral, J. Medina, F. Poulet, H. Dypvik, S. C. Werner, J. L. Vago, F. Rull, *Astrobiology* **2020**, *21*, 307.
- [16] G. Lopez-Reyes, P. Sobron, C. Lefebvre, F. Rull, *Am. Mineral.* **2014**, *99*, 1570.
- [17] J. A. Manrique-Martinez, G. Lopez-Reyes, A. Alvarez-Perez, T. Bozic, M. Veneranda, A. Sanz-Arranz, J. Saiz, J. Medina-Garcia, F. Rull-Perez, *J. Raman Spectrosc.* **2020**, *51*, 1702.
- [18] E. A. Lalla, A. Sanz-Arranz, G. Lopez-Reyes, A. Sansano, J. Medina, D. Schmanke, G. Klingelhofer, J. A. Rodríguez-Losada, J. Martínez-Frías, F. Rull, *Adv. Sp. Res.* **2016**, *57*, 2385.
- [19] E. Lalla, A. Sansano, A. Sanz, R. Navarro, G. Lopez, G. Venegas, J. A. Rodríguez Losada, J. Medina Garcia, J. Martínez-Frías, F. Rull, *Macla* **2011**, *15*, 119.
- [20] E. Lalla, A. Sanz-Arranz, G. Lopez-Reyes, K. Cote, M. Daly, M. Konstantinidis, J. A. Rodríguez-Losada, G. Groemer, J. Medina, J. Martínez-Frías, F. Rull-Pérez, *Life Sci. Sp. Res.* **2019**, *21*, 49.
- [21] E. A. Lalla, G. Lopez-Reyes, A. D. Lozano-Gorrín, F. Rull, *Vib. Spectrosc.* **2019**, *101*, 10.
- [22] E. A. Lalla, M. Konstantinidis, G. Lopez-Reyes, M. G. Daly, M. Veneranda, J. A. Manrique, G. Groemer, J. L. Vago, F. Rull, *J. Raman Spectrosc.* **2020**, *51*, 2525.
- [23] M. Konstantinidis, E. A. Lalla, M. G. Daly, G. Lopez-Reyes, J. M. Stromberg, K. Cote, E. A. Cloutis, *Icarus* **2021**, *358*, 114113.
- [24] E. A. Lalla, G. Lopez-Reyes, A. Sansano, A. Sanz-Arranz, J. Martínez-Frías, J. Medina, F. Rull-Pérez, *Geosci. Front.* **2016**, *7*, 673.
- [25] M. Veneranda, J. Sáiz, A. Sanz-Arranz, J. A. Manrique, G. Lopez-Reyes, J. Medina, H. Dypvik, S. C. Werner, F. Rull, *J. Raman Spectrosc.* **2020**, *51*, 1731.
- [26] M. Veneranda, G. Lopez-Reyes, J. Saiz, J. A. Manrique-Martinez, A. Sanz-Arranz, J. Medina, A. Moral, L. Seoane, S. Ibarria, F. Rull, *Sci. Rep.* **2021**, *11*, 1461.
- [27] G. Lopez-Reyes, J. Saiz, A. Guzman, A. Moral, C. Perez, F. Rull, J. A. Manrique, J. Medina, *European Planetary Science Congress* **2018**, *12*, 1132.
- [28] J. Saiz, G. Lopez-Reyes, M. Veneranda, J. A. Manrique, A. Guzmán, D. Moreno-Dominguez, S. Werner, F. Poulet, J. Medina, F. Rull, *Geophys. Res. Abstracts* **2019**, *21*, 17904.
- [29] M. Veneranda, A. Sanz-Arranz, J. A. Manrique, J. Saiz, C. Garcia-Prieto, E. Pascual-Sánchez, J. Medina, M. Konstantinidis, E. Lalla, A. Moral, L. M. Nieto, F. Rull, G. Lopez-Reyes, *J. Raman Spectrosc.* **2021**. This issue
- [30] R. L. McCreery, *Raman Spectroscopy for Chemical Analysis*, John Wiley & Sons, Inc., New York **2000**.

How to cite this article: G. Lopez-Reyes, M. Veneranda, J. A. Manrique, Á. González Martín, A. Moral, C. Perez-Canora, J. A. Rodríguez Prieto, A. Sanz Arranz, J. Saiz Cano, E. Lalla, M. Konstantinidis, O. Prieto-Ballesteros, J. Medina, M. Á. González, E. Charro, J. M. Lopez, F. Rull, *J Raman Spectrosc* **2021**, *1*. <https://doi.org/10.1002/jrs.6281>